SNP associations are replicated across populations. Replication of association signals is the sine qua non of association studies, and the fact that we observe this even between diverse populations and with small sample sizes highlights the relevance and robustness of the associations we detect. Gene expression is the basis for many crucial functions in the cell, so the relative contribution of these two types of variants is an indication of the nature of the mutational and natural selection processes that contribute to phenotypic diversity and divergence. It is, therefore, essential that we interrogate both SNPs and CNVs (of all types) to perform a comprehensive exploration of genetic effects on phenotypic variation and disease. It is possible that, if a larger number of SNPs were analyzed or a higher resolution of CNVs was available, we would observe more overlap between the effects attributed to CNVs and SNPs. However, the difficulty of designing robust SNP genotyping assays in structurally dynamic regions of the genome (26) suggests that even with more comprehensive interrogation of SNPs and CNVs, the overlap may not be high enough for one type of variation to be sufficient for exploring the genetic causes of disease. We have also demonstrated that it is not necessary to perform such studies with CNV calls or CNV genotypes, but it is possible to use filtered CGH $\log_2$ ratios or any other type of high-quality quantitative signal that reflects underlying CNV. It has also become apparent that there are many more structural variants that contribute to phenotypic variation than our stringent criteria for what is a CNV reveal and that higher-resolution methods are necessary to elucidate their structure and function. Last, but not least, is the fact that we have only considered simple models of association in small samples, so it is very likely that if we apply more complex and realistic models (e.g., epistatic interactions) and/or larger population samples, a larger number of effects would be revealed. The results presented here reinforce the idea that the complexity of functionally relevant genetic variation ranges from single nucleotides to megabases, and the full range of the effects of all of these variants will be best captured and interpreted by complete knowledge of the sequence of many human genomes. Until this is possible we need to survey all known types of genetic variation to maximize our understanding of human evolution, diversity, and disease.

References and Notes

1. B. E. Stranger et al., PLoS Genet. 1, e78 (2005).
2. V. G. Cheung et al., Nature 437, 1365 (2005).
3. S. Doss, E. E. Schadt, T. A. Drake, A. J. Lusis, Genome Res. 15, 681 (2005).
4. R. B. Brem, L. Kruglyak, Proc. Natl. Acad. Sci. U.S.A. 102, 1572 (2005).
5. J. D. Storey, J. M. Akey, L. Kruglyak, PLoS Biol. 3, e267 (2005).
6. M. F. Oleksiak, J. L. Roach, D. L. Crawford, Nat. Genet. 37, 67 (2005).
7. S. A. Monks et al., Am. J. Hum. Genet. 75, 1094 (2004).
8. E. E. Schadt et al., Nature 422, 297 (2003).
9. E. J. Chesler et al., Nat. Genet. 37, 233 (2005).
10. L. Bystrykh et al., Nat. Genet. 37, 225 (2005).
11. E. T. Dermitzakis, B. E. Stranger, Mamm. Genome 17, 503 (2006).
12. T. Pastinen, T. J. Hudson, Science 306, 647 (2004).
13. International HapMap Consortium, Nature 437, 1299 (2005).
14. L. Feuk, C. R. Marshall, R. F. Wintle, S. W. Scherer, Hum. Mol. Genet. 15 (suppl. 1), R57 (2006).
15. A. J. Iafrate et al., Nat. Genet. 36, 949 (2004).
16. J. Sebat et al., Science 305, 525 (2004).
17. E. Tuzun et al., Nat. Genet. 37, 727 (2005).
18. S. A. McCarroll et al., Nat. Genet. 38, 86 (2006).
19. D. F. Conrad, T. D. Andrews, N. P. Carter, M. E. Hurles, J. K. Pritchard, Nat. Genet. 38, 75 (2006).
20. P. Stankiewicz, in Genomic Disorders: The Genomic Basis of Disease, J. R. Lupski, P. Stankiewicz, Eds. (Humana Press, Totowa, NJ, 2006), pp. 357–369.
21. D. A. Kleinjan, V. van Heyningen, Am. J. Hum. Genet. 76, 8 (2005).
22. M. J. Somerville et al., N. Engl. J. Med. 353, 1694 (2005).
23. J. A. Lee et al., Ann. Neurol. 59, 398 (2006).
24. D. P. Locke et al., Am. J. Hum. Genet. 79, 275 (2006).
25. D. A. Hinds, A. P. Kloek, M. Jen, X. Chen, K. A. Frazer, Nat. Genet. 38, 82 (2006).
26. R. Redon et al., Nature 444, 444 (2006).
27. GENEVAR—GENe Expression VARiation, www.sanger.ac.uk/genevar.
28. International HapMap Project, www.hapmap.org; release 16c.1.
29. The Copy Number Variation (CNV) Project Data Index, www.sanger.ac.uk/humgen/cnv/data.
30. R. W. Doerge, G. A. Churchill, Genetics 142, 285 (1996).
31. G. Merla et al., Am. J. Hum. Genet. 79, 332 (2006).
32. We thank A. Clark and J. Pritchard for comments on earlier versions of the manuscript; M. Smith for assistance with software development; and M. Gibbs, J. Orwick, and C. Gerringer for technical support. Funding was provided by the Wellcome Trust to E.T.D., M.E.H., P.D., C.T.S., and N.C.; NIH to E.T.D. and S.T.; Cancer Research U.K. to S.T. and N.T.; the Leukemia and Lymphoma Society and the Brigham and Women's Hospital Department of Pathology to C.L.; and the U.K. Medical Research Council (MRC) to M.D. S.T. is a Royal Society Wolfson Research Merit Award holder. S.W.S. is supported by grants from Genome Canada/Ontario Genomics Institute and is a Scholar of the Canadian Institutes of Health Research and the Howard Hughes Medical Institute.

Evidence That Focal Adhesion Complexes Power Bacterial Gliding Motility

Tâm Mignot,[1]* Joshua W. Shaevitz,[2] Patricia L. Hartzell,[3] David R. Zusman[1]*

The bacterium *Myxococcus xanthus* has two motility systems: S motility, which is powered by type IV pilus retraction, and A motility, which is powered by unknown mechanism(s). We found that A motility involved transient adhesion complexes that remained at fixed positions relative to the substratum as cells moved forward. Complexes assembled at leading cell poles and dispersed at the rear of the cells. When cells reversed direction, the A-motility clusters relocalized to the new leading poles together with S-motility proteins. The Frz chemosensory system coordinated the two motility systems. The dynamics of protein cluster localization suggest that intracellular motors and force transmission by dynamic focal adhesions can power bacterial motility.

During the exhibition of gliding motility, bacteria move across solid surfaces without the use of flagella (1). Gliding motility is important for biofilm formation and bacterial virulence. Motility in *Myxococcus xanthus*, a Gram-negative rod-shaped bacterium, relies on two separate but coordinated motility engines. S motility is powered by type IV pili that are assembled at the leading cell pole; movement is produced as the pili bind to surface exopolysaccharides and are retracted, thereby pulling the cell forward (2). A motility, on the other hand, is not associated with pili or other obvious structures and is not well understood.

To investigate the A-motility system, we studied AglZ, a protein that is essential for A motility but dispensable for S motility (fig. S1, A and B) (3). AglZ is similar to FrzS, an S-motility protein that oscillates from one cell pole to the other when cells reverse direction (4) (fig. S1A). To track the localization of AglZ in moving cells, we constructed an *M. xanthus* strain containing a chimeric *aglZ-yfp* gene in place of the endogenous *aglZ* gene (fig. S2A). This chimeric gene encodes an AglZ–yellow fluorescent protein (YFP) fusion protein that was stable and functional (fig. S2, B and C). We followed AglZ-YFP localization using time-lapse video microscopy: In fully motile cells, AglZ-YFP was localized in

[1]Department of Molecular and Cell Biology, University of California, Berkeley, CA 94720, USA. [2]Department of Integrative Biology, University of California, Berkeley, CA 94720, USA. [3]Department of Microbiology, Molecular Biology, and Biochemistry, University of Idaho, Moscow, ID 83844, USA.

*To whom correspondence should be addressed. E-mail: tmignot@berkeley.edu (T.M.); zusman@berkeley.edu (D.R.Z.)

ordered clusters spanning the cell length; in stalled cells, it was localized at the leading cell pole (fig. S3).

To study the link between the localization of AglZ-YFP and motility, we focused our observations on AglZ-YFP in fully motile cells. These

cells showed an ordered array of AglZ-YFP clusters spanning the cell body (Fig. 1A). As cells moved forward, AglZ-YFP clusters maintained fixed positions with respect to the agar substrate rather than to their relative positions in the cell (Fig. 1A). We analyzed the clusters by taking line scans of the fluorescence intensity along motility paths for successive movie frames (Fig. 1B). To identify the position of peaks in multiple frames, we calculated a thresholded line-scan average (Fig. 1B) (5). This analysis not only located the positions of clusters shown in Fig. 1A, but also had the sensitivity to find other common peaks that were difficult to identify when viewing images with the eye. In every cell that was examined ($n = 30$), the AglZ-YFP clusters remained fixed relative to the substratum. The only AglZ-YFP clusters that moved relative to the cell body were located at the leading pole, which suggests that new sites were assembled at that pole. The number of clusters per cell was dependent on cell length; clusters were disassembled when they reached the rear half of the cell (fig. S4).

We calculated the autocorrelation function of the line-scan averages from six different moving cells (Fig. 1C). Autocorrelations are useful for finding repeating patterns in a signal, such as the determination of the presence of periodicities buried under noise. The average of all six auto-
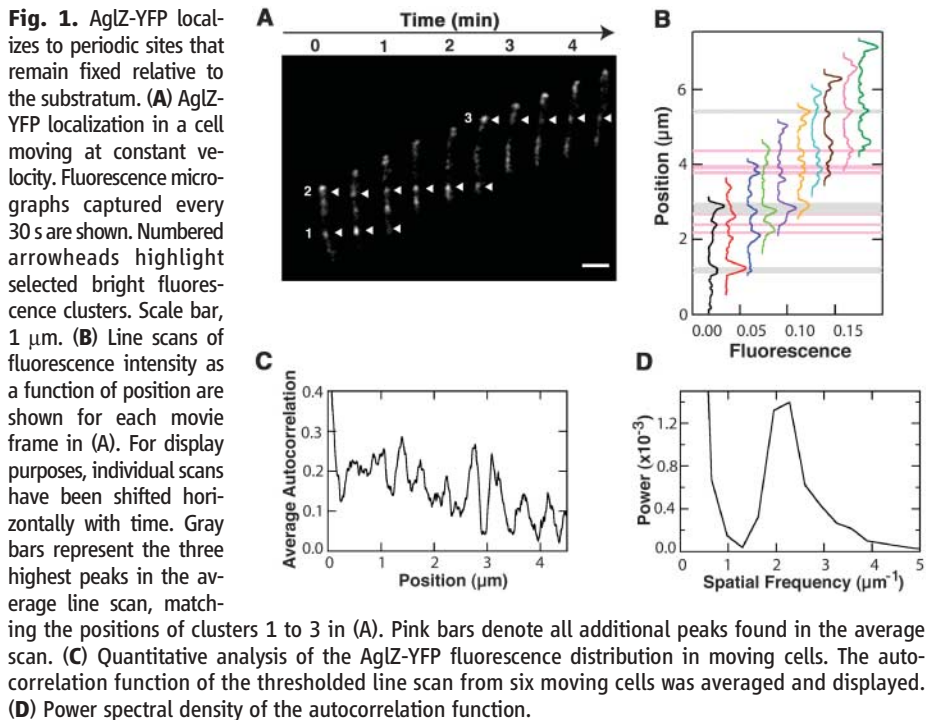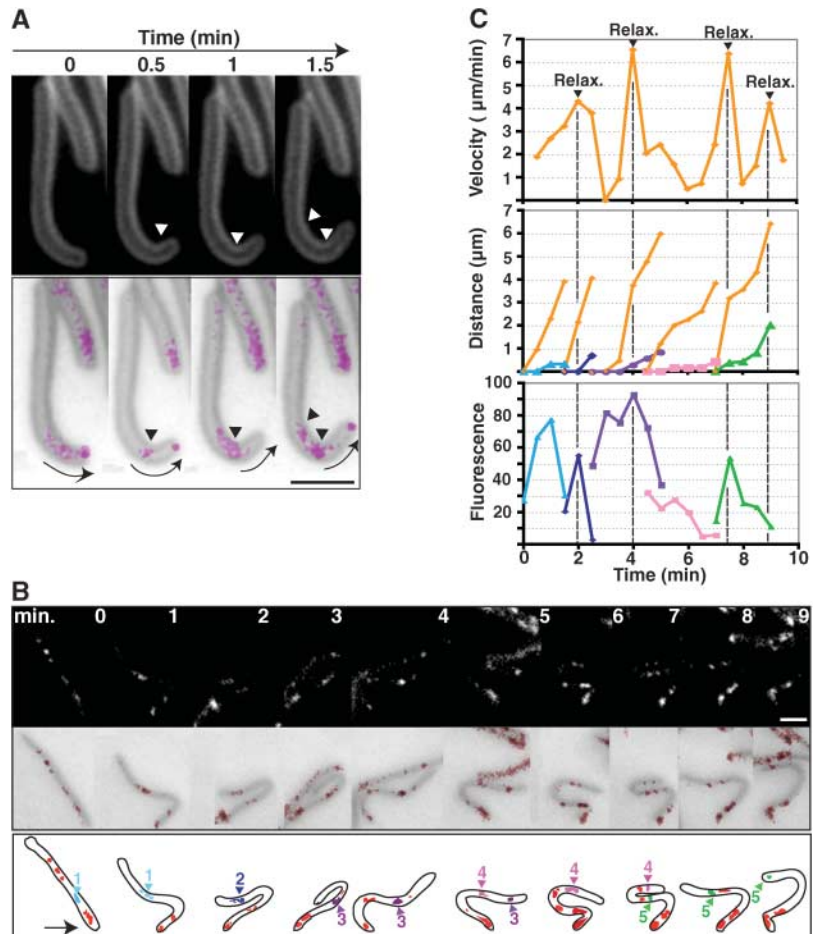

Fig. 1. AglZ-YFP localizes to periodic sites that remain fixed relative to the substratum. (**A**) AglZ-YFP localization in a cell moving at constant velocity. Fluorescence micrographs captured every 30 s are shown. Numbered arrowheads highlight selected bright fluorescence clusters. Scale bar, 1 μm. (**B**) Line scans of fluorescence intensity as a function of position are shown for each movie frame in (A). For display purposes, individual scans have been shifted horizontally with time. Gray bars represent the three highest peaks in the average line scan, matching the positions of clusters 1 to 3 in (A). Pink bars denote all additional peaks found in the average scan. (**C**) Quantitative analysis of the AglZ-YFP fluorescence distribution in moving cells. The autocorrelation function of the thresholded line scan from six moving cells was averaged and displayed. (**D**) Power spectral density of the autocorrelation function.

Fig. 2. AglZ-YFP localizes to transient adhesion sites. (**A**) AglZ-YFP fluorescence clusters in a cell that bends while in motion. (Top) Cells stained with the membrane dye FM4-64 are shown. (Bottom) An overlay of the membrane signal (gray) and the AglZ-YFP signal (magenta), which is artificially colored for better clarity, are shown. White and black arrowheads point to regions of cell-body curvature and localization of the YFP signal, respectively. Arrows indicate the direction of movement. Scale bar, 1 μm. (**B**) AglZ-YFP fluorescence clusters in a cell undergoing flailing motion. Fluorescence and overlaid phase micrographs (top and middle rows, respectively) are shown. Time intervals, 1 min. A cartoon representation (bottom row) shows the clusters numbered and color-coded for the analysis shown in (C). The arrow indicates the stuck leading pole. Scale bar, 2 μm. (**C**) Dynamic behavior of the AglZ-YFP fluorescence clusters in the cell shown in (B). Time intervals, 30 s. (Top) The velocity of the lagging pole over time is shown. Dotted lines mark the times where relaxation of the terminal bend (Relax.) is observed. The leading pole remained immobilized for the entire duration of the time lapse. (Middle) The distance traveled by the AglZ-YFP clusters, color-coded and numbered as in (B), over time is shown. 1, blue triangles; 2, blue diamonds; 3, purple squares; 4, pink squares; 5, green triangles. For each cluster, the distance traveled by the lagging pole (orange diamonds) during the same time interval was plotted to show that the clusters remain mostly fixed relative to the substratum. (Bottom) The relative fluorescence intensity of each cluster over time. The same color code as that used in the middle panel applies.

correlation functions displayed a clear periodicity (Fig. 1C), represented by a single large peak at a spatial frequency of $2.15 \pm 0.03\ \mu m^{-1}$ in its power spectral density (Fig. 1D). This frequency corresponded to a spatial periodicity of 466 ± 7 nm, which is very similar to the helical pitch of bacterial actin MreB as seen in both *Bacillus subtilis* [470 nm (6)] and *Escherichia coli* [460 ± 80 nm (7)].

Because AglZ-YFP clusters remained fixed relative to the substratum as cells moved forward, they must be moving in the opposite direction to that of the cell. These dynamics suggest the formation of cytoskeleton-anchored transient surface adhesions that could power cellular movement. We analyzed cells that bend while in motion to investigate whether AglZ-YFP clusters could indicate sites of transient adhesion between the cell surface and the substratum. First, in a moving cell that was progressively bending, two distinct sites of curvature were observed (Fig. 2A). If AglZ-YFP localizes at sites that mediate adhesion with the substratum, then clusters should accumulate at sites of maximum bending. As expected, accumulation of AglZ-YFP was specifically observed at each site. Second, cells sometimes became stuck at their leading end, which prevented forward movement; these cells bent into U or S shapes as the active A engine pushed against the flexible cell wall. It has been proposed that these flailing motions are due to a motor pushing from the lagging end of the cell (8). However, if multiple motor-coupled adhesion complexes pushed cells forward, flailing would also occur. In that situation, cell bends would form between adhesion complexes. In a flailing cell expressing AglZ-YFP (Fig. 2B), as the front of the cell became fixed, the still-motile cell adopted a right-handed U shape and then relaxed to adopt a left-handed U shape that transitioned into an S shape to become a right-handed U shape again (neighboring cells probably block full relaxation between 2 to 3 min and 8 to 9 min). Cell shape correlated with the pattern of AglZ-YFP clusters. At each bend, enlarged AglZ-YFP fluorescence clusters were not observed at the maximum inflection points, but rather between the bends. The fluorescent clusters maintained relatively fixed positions with respect to the agar substrate, whereas the cell body appeared to move through them (Fig. 2, B and C). Furthermore, as the AglZ-YFP clusters faded and dispersed at the lagging cell pole, terminal cell bends relaxed and a spike in velocity was observed, which suggest that dispersal of the AglZ-YFP clusters indeed removed adhesion constraints (Fig. 2C). Thus, the cell body appears to move through "focal adhesion" sites where AglZ-YFP accumulates.

The dynamics of AglZ-YFP localization (Fig. 1A) suggest that A-engine clusters are assembled at the leading cell pole and disassembled at the lagging end. It follows then that, during cellular reversals, proteins of the A-motility system should be shifted to the new leading pole along with S-motility components (4). Indeed, upon cellular reversal, AlgZ-YFP localized rapidly to the new leading pole (Fig. 3A and table S2). This was a two-step process: Immediately before reversal, the cell paused for 10 s, and AglZ-YFP became diffuse (Fig. 3B). The cell then reversed, and AglZ-YFP
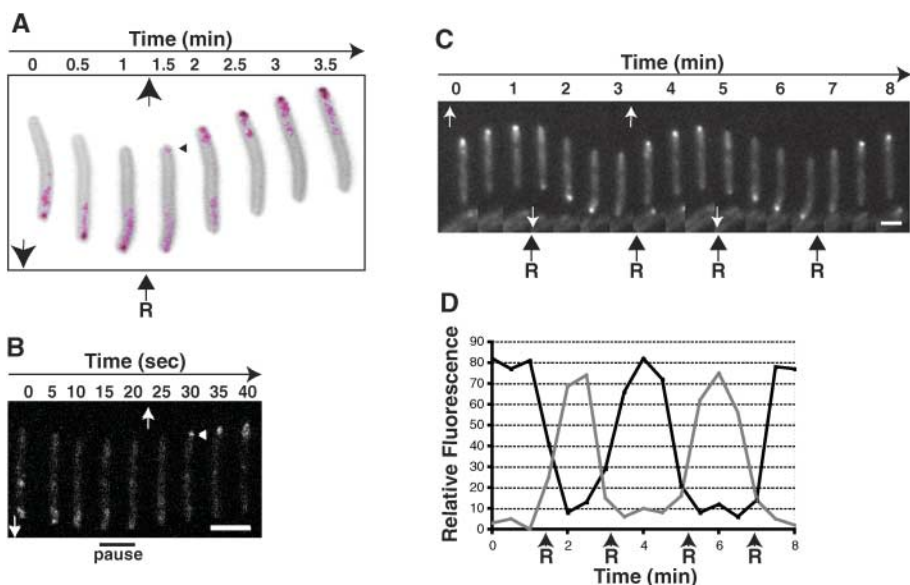

Fig. 3. AglZ-YFP oscillates from pole to pole upon cellular reversals. (**A**) AglZ-YFP localized to the new leading pole upon cellular reversals. Fluorescent micrographs of AglZ-YFP (magenta) and a representative reversing cell stained with FM4-64 (gray) were overlaid to show AglZ-YFP dynamics every 30 s. The black arrows inside the panel indicate the direction of movement. The arrowheads in (A) and (B) show the relocalization of AglZ-YFP at the new leading pole. R, reversal. (**B**) AglZ-YFP dynamics at the time of reversal. Fluorescence micrographs of a reversing cell captured every 5 s are shown. The 10-s delay is indicated by "pause." Scale bar, 2 μm. (**C**) AglZ-YFP oscillations in hyper-reversing cells. Fluorescent micrographs of a *frzCD^c* cell that expresses AglZ-YFP captured every 30 s are shown. The white arrows in (B) and (C) indicate the direction of movement. Scale bar, 2 μm. (**D**) Quantitative fluorescence analysis of the cell presented in (C). The relative fluorescence intensities of each cell pole were measured in arbitrary units and plotted over time. The black line indicates the initial leading pole, and the gray line indicates the initial trailing pole.
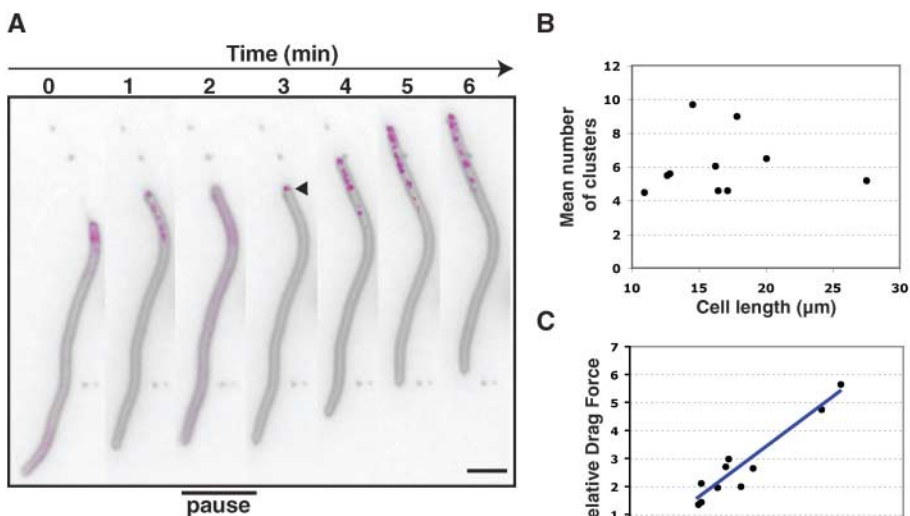

Fig. 4. Dynamics of AglZ-YFP clusters in artificially elongated cells. (**A**) AglZ-YFP dynamics in A$^+$S$^-$-motile filamentous cells. Fluorescent micrographs of a representative 20-μm-long cephalexin-treated cell stained with FM4-64 (gray) expressing AglZ-YFP (magenta). AglZ-YFP is only found distributed over the front part of the cell when the cell is in motion. The arrowhead indicates polar condensation of AglZ-YFP. "Pause" indicates times when the cell motion is stopped. Scale bar, 2 μm. (**B**) Relationship between cluster number and filamentous cell length. (**C**) Relationship between relative drag force overcome and cluster number in filamentous cells.

localized to the new leading pole after a 10-s delay. Thus, AglZ may not trigger polar switching, but rather might be assembled at the new leading pole along with other motility components.

The Frz chemosensory pathway, which regulates cell reversals, controls FrzS translocation to the leading pole when cells reverse direction (4). In a nonreversing *frzE* mutant, AglZ-YFP localization never switched poles. In contrast, a hyper-reversing *frzCD^c* mutant showed very frequent reversals that were always followed by AglZ-YFP polar switching (Fig. 3, C and D, and table S2). In this *frzCD^c* strain, AglZ-YFP was mostly polar in distribution, and ordered intracellular fluorescence clusters were only observed transiently. Thus, cellular reversals result from the concerted switching of both A- and S-motility components to the new leading pole (4). Coordination of these two engines must be achieved through the signaling activity of a common pathway.

Although AglZ-YFP localized to transient adhesion sites, it is unclear whether the force that produces locomotion is generated at those sites. To address this question, we investigated the motility of cells treated with the antibiotic cephalexin. Cephalexin-treated cells, which elongate up to 10 times their natural length, showed almost normal A motility but greatly reduced S motility, which suggests that the A engine is distributed along the cell body whereas the S engine is polar (9). We also observed that 10- to 30-μm-long A^+S^--motile cephalexin-treated cells moved with velocities that were independent of cell length. The localization of AglZ-YFP was also correlated with the activity of the A engine in these cells (Fig. 4A). In these moving filaments, AglZ-YFP was localized in clusters that were distributed in the front part of the cell, whereas the back of the cell was largely depleted of clusters (Fig. 4A); consequently, the number of clusters per cell was largely

independent of cell length (Fig. 4B). Thus, in the filaments, we could test whether force was produced at the sites where AglZ-YFP accumulates by analyzing the relationship between the number of sites and the "drag force overcome" [i.e., the force necessary to power the motility of a cell of given cell length and velocity (5)]. Indeed, the drag force overcome was proportional to the number of clusters in filamentous cells (Fig. 4C), indicating that motility force seems to be produced at the adhesion sites; these characteristics are similar to eukaryotic focal adhesions where both adhesion and force are generated (10).

Previously, a "slime gun" model for gliding motility was proposed because, in several bacterial species, motility is correlated with the secretion of slime through pores (nozzles) located in the outer membrane (11, 12), and a biophysical model suggested that the hydration of slime within the nozzles could generate sufficient force to propel bacteria forward (11). Our results are consistent with an alternate model, whereby intracellular motor complexes that connect to both membrane-spanning adhesion complexes and to the cyto-skeleton power motility by pushing against the substratum and moving the cell body forward, much like focal adhesion–based traction or apicomplexan gliding motility in eukaryotic organisms (fig. S5) (10, 13). The periodicity of the AglZ-YFP clusters strongly implies the existence of a continuous helical filament that spans the length of the cell. Thus, the action of the motor complexes may induce the cell body to rotate as it pulls the cell forward (fig. S5). Rotation of the cell body as cells move has been shown for *Cytophaga* sp., an organism that also secretes slime during motility (14). Slime secretion may be part of the motility system, by supplying additional power for movement and/or adhesion or lubrication of the interface between the cell body

and the substratum (10). The dynamics of AglZ-YFP and FrzS–green fluorescent protein (GFP) fusion protein (4) suggest how the A and S engines might be coordinated: A and S complexes oscillate so that they are targeted together to the new leading pole upon cellular reversal, which is synchronized by the Frz chemosensory system.

References and Notes
1. A. M. Spormann, *Microbiol. Mol. Biol. Rev.* **63**, 621 (1999).
2. Y. Li et al., *Proc. Natl. Acad. Sci. U.S.A.* **100**, 5443 (2003).
3. R. Yang et al., *J. Bacteriol.* **186**, 6168 (2004).
4. T. Mignot, J. P. Merlie, D. R. Zusman, *Science* **310**, 855 (2005).
5. Materials and methods are available as supporting material on *Science* Online.
6. H. J. Defeu Soufo, P. L. Graumann, *BMC Cell Biol.* **6**, 10 (2005).
7. T. Kruse, J. Moller-Jensen, A. Lobner-Olesen, K. Gerdes, *EMBO J.* **22**, 5283 (2003).
8. C. W. Wolgemuth, *Biophys. J.* **89**, 945 (2005).
9. H. Sun, Z. Yang, W. Shi, *Proc. Natl. Acad. Sci. U.S.A.* **96**, 15178 (1999).
10. M. A. Wozniak, K. Modzelewska, L. Kwong, P. J. Keely, *Biochim. Biophys. Acta* **1692**, 103 (2004).
11. C. Wolgemuth, E. Hoiczyk, D. Kaiser, G. Oster, *Curr. Biol.* **12**, 369 (2002).
12. E. Hoiczyk, W. Baumeister, *Curr. Biol.* **8**, 1161 (1998).
13. J. Baum, A. T. Papenfuss, B. Baum, T. P. Speed, A. F. Cowman, *Nat. Rev. Microbiol.* **4**, 621 (2006).
14. S. L. Godwin, M. Fletcher, R. P. Burchard, *J. Bacteriol.* **171**, 4589 (1989).
15. We thank Y. Inclàn for the construction of pZeroΩaglZ and comments on the manuscript; and J. Merlie, R. Losick, and G. Oster for helpful discussions and comments. This research was supported by a grant from NIH to D.R.Z. (GM20509).

Apoptosis Initiated When BH3 Ligands Engage Multiple Bcl-2 Homologs, Not Bax or Bak

Simon N. Willis,[1] Jamie I. Fletcher,[1] Thomas Kaufmann,[1] Mark F. van Delft,[1,2] Lin Chen,[1] Peter E. Czabotar,[1] Helen Ierino,[1] Erinna F. Lee,[1,2] W. Douglas Fairlie,[1] Philippe Bouillet,[1] Andreas Strasser,[1] Ruth M. Kluck,[1] Jerry M. Adams,[1]* David C. S. Huang[1]*†

A central issue in the regulation of apoptosis by the Bcl-2 family is whether its BH3-only members initiate apoptosis by directly binding to the essential cell-death mediators Bax and Bak, or whether they can act indirectly, by engaging their pro-survival Bcl-2—like relatives. Contrary to the direct-activation model, we show that Bax and Bak can mediate apoptosis without discernable association with the putative BH3-only activators (Bim, Bid, and Puma), even in cells with no Bim or Bid and reduced Puma. Our results indicate that BH3-only proteins induce apoptosis at least primarily by engaging the multiple pro-survival relatives guarding Bax and Bak.

Whether a cell dies in response to diverse developmental cues or cellular stresses is determined largely by interactions between three factions of the Bcl-2 protein family (1). Two factions promote apoptosis: The BH3-only proteins (including Bim, Bid, Puma, Bad, and Noxa) sense cellular damage, and Bax and Bak are critical downstream mediators of apo-

ptosis because their combined absence abolishes most apoptotic responses (2, 3). When activated, Bax and Bak permeabilize the outer mitochondrial membrane, freeing proapoptogenic factors such as cytochrome c, which promote activation of the proteases (caspases) that mediate cellular demolition. Activation of Bax and Bak is opposed by the pro-survival faction: Bcl-2, Bcl-x_L, Bcl-w, Mcl-1, and A1. These guardians are inactivated when BH3-only proteins insert their BH3 domain into a groove on the pro-survival proteins (1).

A widely embraced model for the initiation of apoptosis (4) (Fig. 1A) proposes that a subset of BH3-only proteins termed "activators"—namely

[1]The Walter and Eliza Hall Institute of Medical Research, 1G Royal Parade, Parkville, Victoria 3050, Australia. [2]Department of Medical Biology, University of Melbourne, Parkville, Victoria 3010, Australia.

*These authors contributed equally to this work.
†To whom correspondence should be addressed. E-mail: huang_d@wehi.edu.au